Charge excitation spectrum in UPt_3

P. Tran, S. Donovan, and G. Grüner
Department of Physics and Astronomy, University of California, Los Angeles, Los Angeles, California 90095-1547
(Received 12 October 2001; published 22 April 2002)

We report on the observation of a pseudogap, together with a zero-energy mode at low temperatures in the heavy fermion compound UPt_3. The zero-energy mode can be described by an extended Drude response with a frequency-dependent mass and relaxation rate. The spectral weight of this mode is in good agreement with the superconducting penetration depth if the usual sum rule arguments are used. The pseudogap energy, in units of $\hbar\omega/k_B$, is comparable to the temperature where the magnetic correlations develop (at approximately 5 K). Our findings indicate that the magnetic state observed in this material is related to a Fermi-surface instability of the heavy fermion state. We also compare the optical response to the conductivity observed in other heavy fermion compounds with a magnetic ground state.

DOI: 10.1103/PhysRevB.65.205102 PACS number(s): 78.20.−e, 71.27.+a

I. INTRODUCTION

Heavy fermion (HF) metals at low temperatures have attracted wide interest in recent years. The thermodynamic and magnetic properties are usually described in the context of an interacting Fermi liquid (FL), leading to a strongly enhanced specific heat and magnetic (Pauli) susceptibility.[1] These are understood to arise as a consequence of a coherent many-body resonance which appears at the Fermi level.[2] The narrow bandwidth translates into a heavy mass, hence the name heavy fermions. This state is gradually removed by thermal fluctuations, and the temperature scale describing this is usually referred to as the coherence temperature $T_{\rm coh}$.

The transport properties, and in general the electrodynamic response of heavy fermion materials, are fundamentally different from that of a simple metal.[3] The charge excitation spectra are described by the frequency- and temperature-dependent relaxation rate $\Gamma^*(\omega,T)$ and the effective mass $m^*(\omega,T)$.

In this paper, we discuss the optical properties of the archetype heavy fermion compound UPt_3. The material is one of the most studied among the strongly correlated metals. In the coherent regime, the dc resistivity increases as T^2, indicative of electron-electron scattering. The coefficient of this T^2 term is proportional to the square of the specific-heat coefficient, as expected for a Fermi liquid.[4] This then suggests that UPt_3 is a simple renormalized FL at low temperatures and low frequencies. However, various experiments[5–8] which sample the magnetic character of the state, such as neutron scattering, muon spin rotation, and NMR, indicate the progressive development of a magnetic state below about 5 K. The magnetic moment is extremely small, $\mu = 0.02\,\mu_B$, and long-range order cannot be observed. The nature of this state is not well understood and is also not well characterized. There is no firm conclusion about the nature of the ground state, in particular whether the magnetic order is commensurate with the underlying lattice. The appearance of the magnetic moment is in clear conflict with a simple FL description. Moreover, the role of impurities and their contribution to the magnetic characteristics is not established.

Earlier optical experiments[9–13] in this material have established many of the salient features of the HF metals, such as the enhanced electrodynamical mass, enhanced relaxation time, and reduced spectral weight. These experiments, however, did not sample the response at low energies (well below the conventional spectral range where Fourier transform spectroscopy is effective), or they were conducted only at a few selected frequencies and a detailed evaluation of the frequency-dependent response was not possible.

In this paper, we summarize our low-energy optical studies of both polycrystalline and single crystal UPt_3. By conducting careful experiments in the millimeter wave and microwave spectral range, we find, by analyzing both the real and imaginary parts of the optical conductivity $\hat{\sigma}(\omega) = \sigma_1(\omega) + i\sigma_2(\omega)$, that below approximately 5 K a pseudogap develops in the optical spectrum. This gap appears in the same temperature region where magnetic correlations have been observed in this compound, and the magnitude of the gap is comparable to the thermal energy associated with the development of (short range) magnetic correlations. The observation suggests that in this material (and possibly in other compounds where electron-electron correlations are important), the development of a coherent FL state, at a temperature $T_{\rm coh}$, is followed, upon a further decrease of the temperature, by a state where the excitations do not have a simple gapless character. It is conceivable that this state is close to a spin-density-wave state, leading to a pseudogap in the charge excitation spectrum.

We first summarize the experimental technique employed and our experimental results. This is followed by an analysis of the frequency-dependent complex conductivity. The connection of the response in the normal state to the superconducting penetration depth is also established. Finally, we compare our findings on UPt_3 with observations on other HF magnetic metals. Some of our results were published earlier.[14]

II. EXPERIMENTAL RESULTS

Measurements were made on a large polycrystalline UPt_3 ingot ($1\times1\times0.15\,\text{cm}^3$) and on needlelike single crystals (with excellent surface characteristics), both grown by Professor Maple's group at UCSD. We have measured the temperature dependence of the resistivity in both single crystal

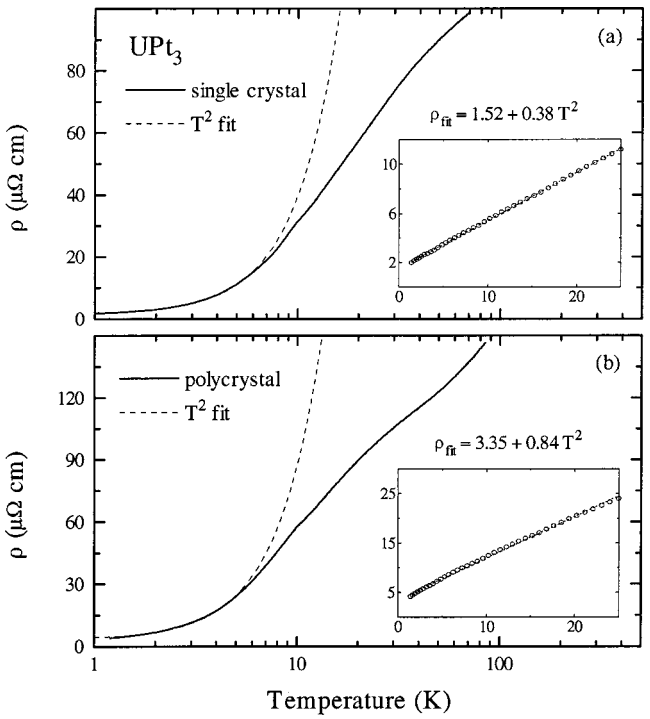

FIG. 1. Temperature dependence of the dc resistivity measured on (a) single crystalline and (b) polycrystalline UPt_3 used in this study. The dashed lines show the T^2 temperature dependence of the dc resistivity, with parameters given on the figure. The insets are the plots of the dc resistivity vs T^2 at low temperatures; the straight-line fits indicate Fermi-liquid behavior.

and polycrystal specimens, and the results are displayed in Fig. 1. Both single-crystal and polycrystal samples display a temperature dependence given by $\rho=\rho_0+AT^2$, with the parameters given in the figure. We find the polycrystalline sample to have a dc resistivity $\rho_{\rm dc}$ of 4 $\mu\Omega$ cm at 1.2 K, somewhat higher than the sample of Ref. 11, but still indicative of the high quality of the sample. The single-crystal samples had a typical resistivity (when extrapolated to $T=0$) of 1.5 $\mu\Omega$ cm along the needle axis. In both cases the resistivity starts to deviate from the quadratic temperature dependence above about 5 K; this is interpreted as the onset of the gradual destruction of the correlated state with increasing temperature.

In order to probe the electrodynamical response of UPt_3 and to evaluate the frequency-dependent complex conductivity $\hat{\sigma}(\omega)=\sigma_1(\omega)+i\sigma_2(\omega)$ over a broad frequency range (0.2–105 $\rm cm^{-1}$), our data, obtained using a variety of different experimental techniques, have been combined. Our results, obtained in the low energy end of the electromagnetic spectrum (the micro and millimeter wave spectral range), have been also combined with the findings obtained by others at higher frequencies; this allows the utilization of the Kramers-Kronig (KK) relations. Previous investigations[9–13] by several different groups have been carried out in the region between 2 $\rm cm^{-1}$ and the ultraviolet (UV) spectral range. We have employed a quasioptical method in the millimeter wave spectral range.[15] This configuration allows an evaluation of both components of the optical conductivity. In the microwave spectral range, most of our experiments employed cavity resonators. In this method, the cavity characteristics (the width and central frequency of the resonance line shape) are measured as a function of temperature both with and without the sample presence. Two different configurations are employed. For the small single-crystalline specimens, the sample is inserted into the resonant cavity at a position of maximum magnetic or electric field. For the polycrystalline specimens, the sample forms part of the resonance structure—usually the end wall of the cavity. The complex surface impedance $Z_s=R_s-iX_s$ of the sample is proportional to the change in the cavity characteristics caused by the introduction of the sample into the cavity or replacing the end wall (R_s is the surface resistance and X_s is the surface reactance). The method and the analysis of the experimental results are fully described in Refs. 16 and 17. These parameters, in turn, can be used to calculate the components of the complex conductivity $\hat{\sigma}(\omega)$ through the relation

$$Z_s=R_s-iX_s=\left(\frac{\mu_0\omega}{4\pi i(\sigma_1+i\sigma_2)}\right)^{1/2} \tag{1}$$

where ω is the measured frequency and μ_0 is the free-space permeability. In order to extract absolute values, we have assumed that above 30 K UPt_3 behaves as a simple metal in the Hagen-Rubens limit [with $\hat{\sigma}(\omega)\approx\sigma_1(\omega)\approx\sigma_{\rm dc}$], where

$$R_s=X_s=\left(\frac{\mu_0\omega\rho_{\rm dc}}{8\pi}\right)^{1/2}, \tag{2}$$

The relatively high resistivity at 30 K leads to a short relaxation time justifying this assumption. Our data for polycrystalline UPt_3, as shown in Fig. 2, were normalized at 30 K using the dc resistivity obtained from a small slice of the same ingot.

Two types of resonators were employed: enclosed metallic resonators[17] and so-called composite resonators.[18] At frequencies of 2.0, 3.3, and 5.0 $\rm cm^{-1}$, the UPt_3 ingot was used as the end plate of a TE_{011} enclosed resonator with an unloaded low-temperature quality factor of $Q=10^4$. At lower frequencies, the enclosed resonators are large, and become impractical. We have developed cavities, which we call composite resonators, where part of the enclosed structure is filled with a high-dielectric-constant medium. (As, broadly speaking, the size of the resonant structure is proportional to $\varepsilon^{-1/2}$, where ε is the dielectric constant of the dielectric which fills the cavity, a significant reduction of the size of the resonator can be achieved). Consequently, the end-plate configuration can be extended to low frequencies. We have used this method at frequencies of 0.25, 0.47, and 1.2 $\rm cm^{-1}$.

Surface roughness is known to enhance the surface impedance, and has to be corrected for.[19] This was taken into account by using two different approaches. A reference run was made at each frequency by evaporating several microns of Au onto the surface of the ingot and remeasuring. We found that the cavity Q with the Au-covered sample was approximately 50% lower than with a smooth Cu end plate; we attribute the reduction of the cavity Q to the surface

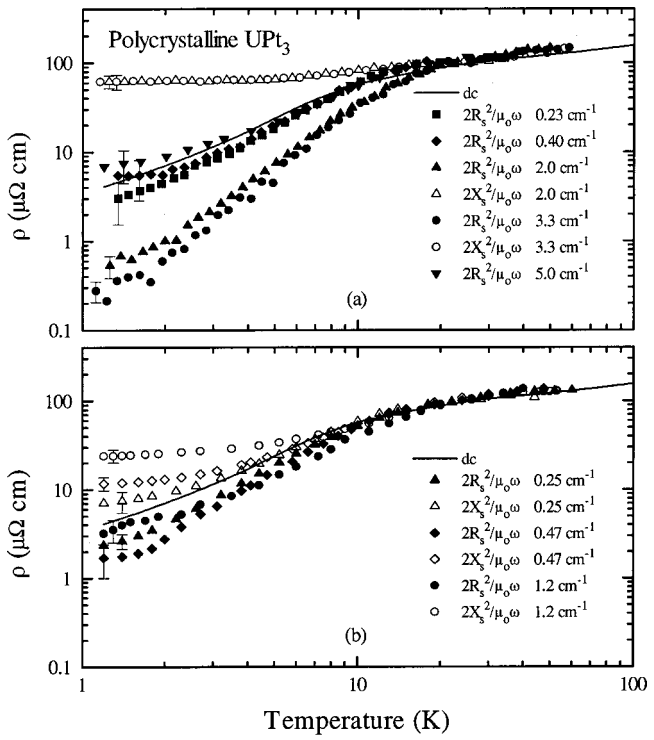

FIG. 2. Temperature dependence of ρ_{dc} (solid line) together with the resistivities calculated from the microwave surface resistance and reactance ($2R_s^2/\omega\mu_0$ and $2X_s^2/\omega\mu_0$, respectively) of polycrystalline UPt_3. The data were obtained from two different experimental arrangements: (a) enclosed resonators, and (b) composite resonators. The data at 5.0 cm^{-1} were taken from Ref. 12. The data were normalized to the dc resistivity by assuming that, above 30 K, UPt_3 behaves as a simple metal in the Hagen-Rubens limit.

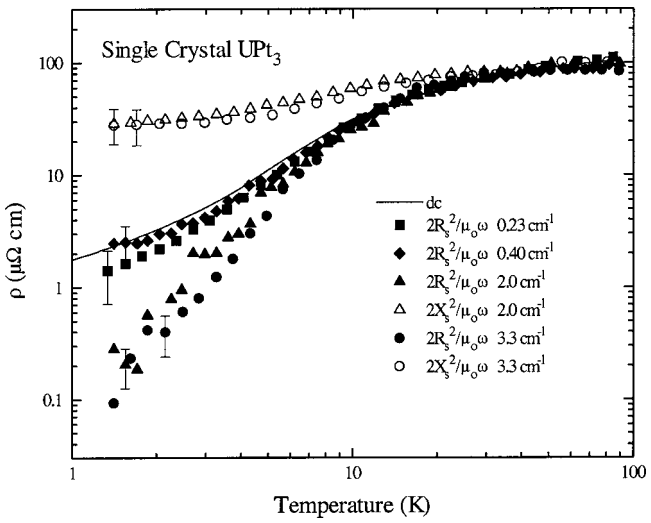

FIG. 3. Temperature dependence of ρ_{dc} together with, $2R_s^2/\omega\mu_0$ and $2X_s^2/\omega\mu_0$ measured on single-crystalline UPt_3, using the enclosed resonator arrangement. The data refer to the measurements with the microwave electric field along the highly conducting c direction. Both the surface resistance and surface reactance were normalized at high temperature (above 30 K) by assuming that the Hagen-Rubens limit applies.

roughness of our polycrystalline sample. A detailed comparison of the results of Ref. 12, obtained on the same ingot as measured here, indicates that we have obtained a somewhat lower value of R_s than previously found. We attribute this discrepancy to the fact that the previous data were analyzed using a Cu end plate reference run, and the additional losses associated with the surface roughness of the sample were improperly attributed to the intrinsic behavior of UPt_3. A reanalysis of Awasthi *et al.*'s data[12] at 3.3 cm^{-1} was made and compared with our results at the same frequency. We find that, within the experimental error, the two sets of data give identical results. The same reanalysis of Awasthi *et al.*'s data was made at 5 cm^{-1}, and the results are also shown in Fig. 2. Alternatively, we have assumed that surface roughness leads to an additional, temperature-independent loss, which has been evaluated as follows. Again, we assume that above 30 K UPt_3 is in the Hagen-Rubens limit. Without a contribution to the loss due to surface roughness, the change of the width versus $\rho_{dc}^{1/2}$ is expected to be a straight line intercepting the origin. We find that our results above 30 K, when plotted against $\rho_{dc}^{1/2}$, give a straight line, though with a finite intercept for $\rho_{dc}^{1/2}$ extrapolated to zero. We believe this value represents the contribution of the surface roughness to the loss, and have used this value in correcting our results. The same procedure is applied to correct for the frequency shift. Employing an *in situ* perturbation technique,[16] we have measured Z_s of the small needlelike single crystals of UPt_3 by placing the needle axis along the maximum electric field. The data are displayed in Fig. 3. Due to the excellent surface characteristics, no correction for the surface roughness is needed.

Two different and complementary methods were used to extract the components of the frequency-dependent conductivity from the measured surface impedance data. The first method is based on an evaluation of the absorptivity $A(\omega)$ from the surface resistance. For conducting samples with R_s, $X_s \ll Z_o$, where $Z_o = 377\ \Omega$ is the impedance of free space, and the absorptivity $A(\omega)$ is simply related to R_s by the relation[20]

$$A(\omega) = 1 - R(\omega) \approx \frac{4R_s}{Z_o}. \tag{3}$$

As both R_s and X_s are much smaller than Z_o for UPt_3 at all temperatures investigated, we can combine our results with the results from previous measurements. At 1.2 K, all of the results are displayed in Fig. 4(a). Data obtained at different temperatures are displayed in Fig. 4(b). An additional reflectivity measurement was carried out between 7 and 13 cm^{-1} in the submillimeter spectral range using a coherent source spectrometer,[19] and the results are also displayed in Fig. 4. Within experimental uncertainty, the results of this nonresonant measurement are temperature independent below 20 K. These data are consistent with previous absorptivity measurements.[11,12]

At each temperature, we have made an interpolation between the measured points, as shown in Fig. 4, and have used these values, together with suitable extrapolations at both low and high frequencies, to make a KK transformation

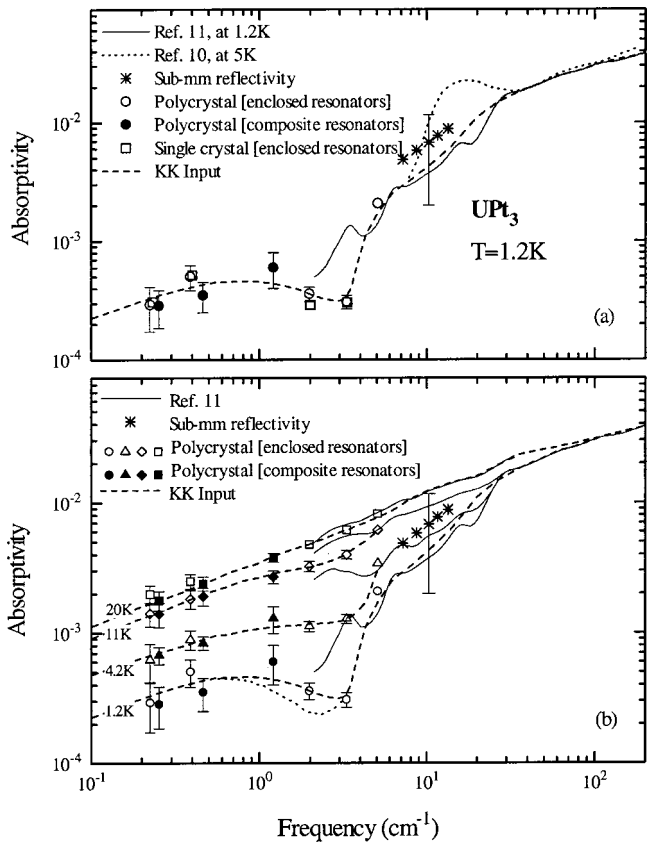

FIG. 4. (a) absorptivity $A(\omega)$ measured at 1.2 K by various techniques. The solid and dotted lines are the optical absorptivity data taken from Refs. 10 and 11. The open and solid symbols are the results of the microwave cavity measurements, calculated from R_s values shown in Figs. 2 and 3. Data displayed by asterisks are taken from the submillimeter reflectivity measurements at 4.2 K (Ref. 14). The dashed line is an interpolation used to calculate the conductivity through the KK relation. (b) absorptivity $A(\omega)$ measured between 1.2 and 20 K. The dashed lines are the interpolations used in the KK analysis. The solid lines are again the optical absorptivity data taken from Refs. 10 and 11.

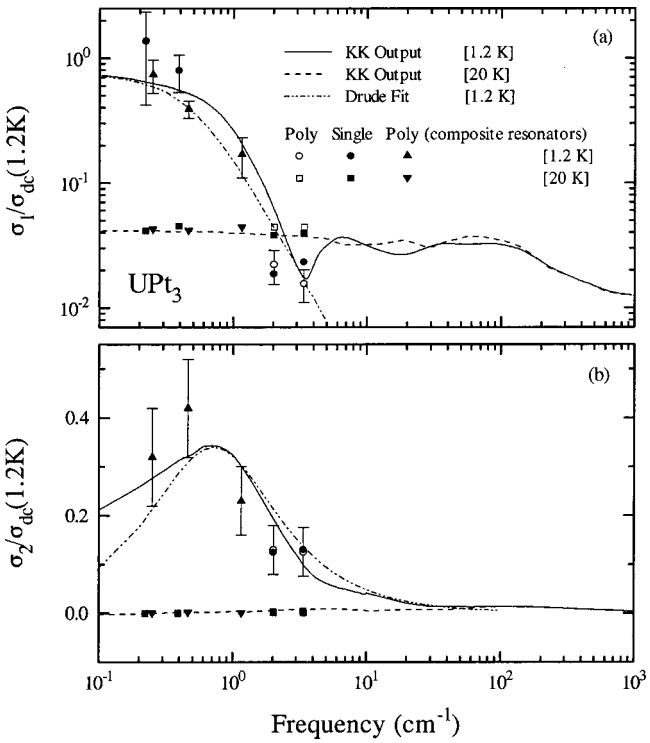

FIG. 5. The complex optical conductivity of UPt_3. The solid and dashed lines are the results of the KK calculations at 1.2 and 20 K, respectively. The displayed data points (at 0.25, 0.47, 1.2, 2.0, and 3.3 cm^{-1}) are conductivity values calculated directly from R_s and X_s. The dash-dotted lines are the Drude fit to the low-frequency part of the 1.2-K spectrum, using a frequency-independent scattering rate. (a) The real parts of the optical conductivity $\sigma_1(\omega)$ at 1.2 and 20 K, normalized to the dc resistivity at 1.2 K [2.5×10^5 and 6.5×10^5 Ω^{-1} cm^{-1} for polycrystalline and single-crystalline samples, respectively]. (b) The imaginary parts of the optical conductivity $\sigma_2(\omega)$, which are also normalized to the dc resistivity at 1.2 K. The symbols refer to both (a) and (b).

of $A(\omega)$. In Fig. 5, we display $\sigma_1(\omega)$ and $\sigma_2(\omega)$ at 1.2 and 20 K, normalized to the dc conductivity at 1.2 K.

The second method of evaluating the two components of the optical conductivity $\sigma_1(\omega)$ and $\sigma_2(\omega)$ utilizes both R_s and X_s, and is based on Eq. (1), which establishes the relation between the components of the surface impedance and conductivity. Due to the thermal expansion, at frequencies 0.23 and 0.4 cm^{-1}, we were unable to measure X_s of the single crystal, and the values of σ_1 which are shown in Fig. 5 are calculated assuming that $R_s=X_s$; the Hagen-Rubens relation given in Eq. (2). This is a reasonable assumption, as will be discussed later.

III. DISCUSSION

We first note that the frequency-dependent absorptivity is different from that of the renormalized Drude metal. In particular, the absorptivity shown in Fig. 4 displays a well-defined minimum near 3 cm^{-1}. Such a minimum is the signature of the development of a pseudogap. This pseudogap is also clearly evident in the frequency dependence of the conductivity $\sigma_1(\omega)$, displayed in Fig. 5. This gap feature gradually disappears with increasing temperature; it is not evident above 5 K, and at 20 K the conductivity is observed to be essentially independent of frequency.

Before discussing the implications of our findings, we comment on the reliability of the analysis procedures we have employed. Both methods of evaluation of $\sigma_1(\omega)$ lead to a pseudogap in the millimeter wave spectral range. This is well established as a result of the increase of $\sigma_1(\omega)$ below about 1 cm^{-1}, by the strong decrease of $\sigma_1(\omega)$ at 2.0 and 3.3 cm^{-1} as the temperature is lowered to 1.2 K, and by the weak temperature dependence at higher frequencies. The KK analysis also leads to a pseudogap—$A(\omega)$ directly evident from, which displays a minimum near 3 cm^{-1} followed by sharp rise at higher frequencies. However, within our experimental uncertainties, the precise shape of this pseudogap is undetermined due to the difficulties associated with the KK analysis, where interpolations have to be used between the data points available at fixed frequencies. Next we discuss

the two salient features we observe: the zero energy mode and the pseudogap.

A. Zero-energy mode

In the single-band model at $T=0$ K, where the free carriers are undergoing frequency-dependent scattering, the complex conductivity $[\hat{\sigma}(\omega)=\sigma_1(\omega)+i\sigma_2(\omega)]$ may be written in the form of an extended Drude conductivity

$$\hat{\sigma}(\omega)=\frac{\omega_p^2}{4\pi}\frac{1}{\Gamma(\omega)-i\omega[m^*(\omega)/m_b]}, \tag{4}$$

where $\omega_p=2\pi\nu_p$ is the angular unscreened optical plasma frequency, and $m_b=3.7m_e$ is the optical band mass (m_e is the free-electron mass).[11] The frequency-dependent scattering rate $\Gamma(\omega)$ and effective mass $m^*(\omega)$ can be expressed in terms of σ_1 and σ_2 as follows:

$$\Gamma(\omega)=\frac{\omega_p^2}{4\pi}\cdot\frac{\sigma_1(\omega)}{[\sigma_1(\omega)]^2+[\sigma_2(\omega)]^2}, \tag{5a}$$

$$\frac{m^*(\omega)}{m_b}=\frac{\omega_p^2}{4\pi}\cdot\frac{\sigma_2(\omega)/\omega}{[\sigma_1(\omega)]^2+[\sigma_2(\omega)]^2}. \tag{5b}$$

A Drude fit to the zero-energy mode of the conductivity (Fig. 5a), using a frequency-independent scattering rate Γ, gives $\nu_p=2.4$ eV, $\Gamma=32.5$ cm^{-1}, and $m^*/m_b=65$.

At finite temperature, using the measured temperature-dependent conductivity, one can calculate the temperature-dependent effective mass and relaxation rate, as displayed in Fig. 6. The temperature dependence of the mass indicates a gradual removal of the enhancement effects with increasing temperature. Taking the temperature where the mass decreases by a factor of 2 from its zero-temperature value leads to a characteristic temperature, which we associate with the coherent temperature ($T_{\rm coh}$) of approximately 15 K. This value is in broad agreement with the values derived from the temperature dependence of the thermodynamic quantities.[21]

With the conductivities $\sigma_1(\omega)$ and $\sigma_2(\omega)$ at 1.2 K, as evaluated from R_s and X_s, Eq. (5) gives enhanced masses of $m^*/m_e=254$, 260, and 247 at frequencies of 0.25, 0.47, and 1.2 cm^{-1}, respectively, as shown in Fig. 6. These results suggest that, within experimental uncertainties, m^* is frequency independent in this energy range. Furthermore, below 5 K m^* is also temperature independent. For a Fermi liquid, at low temperatures and frequencies, the effective mass is, to a good approximation, independent of temperature and frequency while the temperature and frequency dependence of the relaxation rate are given by[22]

$$\Gamma=A(k_BT)^2+B(\hbar\omega)^2+\Gamma_0, \tag{6}$$

where A and B are the temperature- and frequency-independent coefficients, and Γ_0 is the relaxation rate due to impurity scattering. Using the unscreened plasma frequency $\nu_p=2.4$ eV and the dc residual resistivity $\rho_0=3.35\ \mu\Omega$ cm [from Fig. 1(b)], the calculated value for Γ_0 is 20.9 cm^{-1}. The electron-electron scattering process should lead to a general relation between the coefficients A and B. Within the framework of FL theory, the ratio A/B is $(2\pi)^2$ for electron-electron scattering processes.[23] Our experimental result, from Fig. 6(a), gives a ratio A/B of 0.31 at 0.25 cm^{-1}.

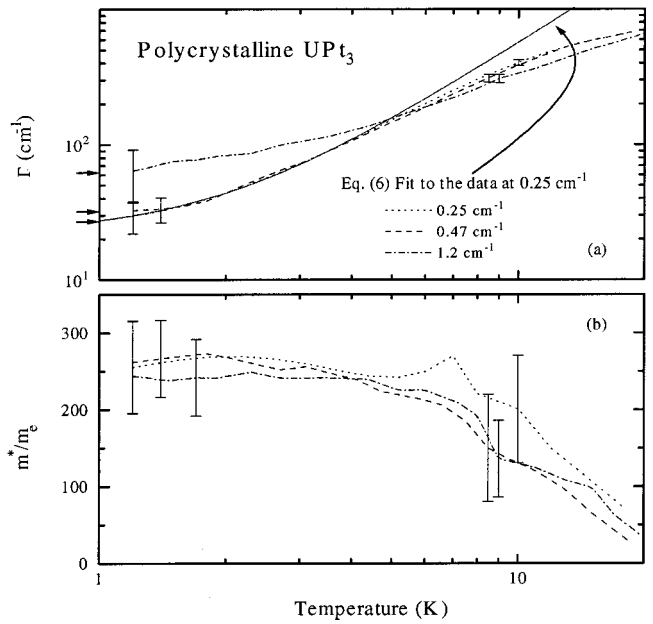

FIG. 6. (a) The temperature dependence of the relaxation rate Γ in polycrystalline UPt_3, as measured at 0.25, 0.47, and 1.2 cm^{-1} (displayed by the dotted, dashed, and dash-dotted lines), together with the T^2 fit to the data at 0.25 cm^{-1} (solid line). The marking arrows on the left axis show the zero-temperature extrapolations at different frequencies, and indicate the strong frequency-dependence of Γ at low temperatures. (b) The temperature dependence of the renormalized effective mass. Note that m^*/m_c is approximately independent of the temperature below 5 K, where the relaxation rates display a T^2 temperature dependence. The symbols refers to both (a) and (b).

As shown in Fig. 7, our experimental result at 1.2 K yield the A/B ratio of 0.37. These results are in clear disagreement with the value $(2\pi)^2$ predicted from FL theory. Next we discuss the spectral weight of the zero-energy mode.

$$\int_0^\infty \sigma_1(\omega)d\omega=\frac{\pi ne^2}{2m^*}\equiv\frac{(\omega_p^*)^2}{8}, \tag{7}$$

where $\omega_p^*=\sqrt{4\pi ne^2/\mathrm{m}^*}$ is the renormalized plasma frequency, and $n=1.5\times10^{22}$ cm^{-3} is the carrier density derived from Hall measurements.[24] Assuming all the electrons participate in this mode, the number of carriers (from the Hall measurements) leads to a strongly enhanced effective mass of $m^*=300\mathrm{m}_e$ at 1.2 K. This is in excellent agreement with the effective mass as evaluated from the surface impedance measurements directly [using Eq. (5)]. This value of the effective mass can be compared with the enhanced thermodynamic mass,[24] of $m^*\leqslant400m_e$, establishing a clear relation between the thermodynamics and electrodynamics of the HF state. Such an overall correspondence has been found earlier for a variety of HF compounds.[3]

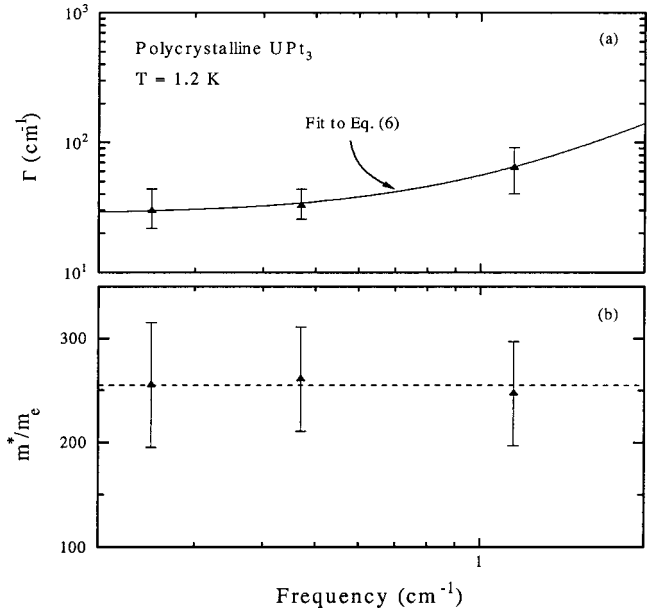

FIG. 7. (a) The frequency-dependent scattering rate at 1.2 K, at frequencies below the pseudogap region. The full line is a fit to the data using Eq. (6). (b) The frequency dependence of the effective mass in the same spectral range. The dashed line through the data points indicates a frequency-independent effective mass.

The spectral weight can be related to the superconducting properties through the well-known Tinkham-Ferrell sum rule.[25] The London penetration depth λ is given by

$$\lambda(T=0)=\frac{c}{\sqrt{8\int_0^\infty \Delta\sigma_1(\omega)d\omega}}, \tag{8}$$

where $\Delta\sigma_1(\omega)$ is the difference between the conductivity observed in the metallic and superconducting states. Assuming a weak-coupling superconductivity, the transition temperature[26] of 0.7 K translates into a superconducting gap of 1.5 cm^{-1}. The inverse renormalized relaxation time $1/\tau$ is smaller than the superconducting gap, placing UPt_3 in the clean limit. In this limit, Eq. (8) reduces to

$$\lambda(T=0)=\frac{c}{\omega_p^*}. \tag{9}$$

The renormalization of the London penetration depth has been derived by Varma *et al.*,[27] and their conclusion is in agreement with Eq. (9). Using the value of ω_p^* as established before, we arrive at $\lambda(T=0\ \mathrm{K})=7000$ Å. This value is in excellent agreement with the value measured directly, $\lambda=6000-7000$ Å.[28]

B. Finite-energy charge excitation

As described in Sec. III A, the zero-energy mode of the optical conductivity at 1.2 K can be fitted to an extended Drude form. Above 3 cm^{-1}, the optical conductivity at 1.2 K has a gaplike feature. We note that the broad maximum observed around 7 cm^{-1} is different from what is observed for a three-dimensional semiconductor[29] (where the conductivity increases as $[\hbar\omega-\Delta]^{1/2}$ above the gap Δ). The feature we observe is instead reminiscent of what is expected for a spin-density state,[30] or a nearly one-dimensional metallic state[31] which can be described in terms of the Hubbard model near half-filling. Both lead to a conductivity which is given by $\sigma_1(\omega)\sim[\hbar\omega-\Delta]^{-1/2}$ near to the gap. Instead of a well-defined square root singularity at the gap, here we observe a somewhat broadened feature with a finite conductivity below the maximum. These features would suggest a pseudogap, in contrast to a fully developed gap, in the charge excitation spectrum. This pseudogap conductivity can be fitted to the conductivity of a one-dimensional semiconductor, $[\hbar\omega-\Delta]^{-1/2}$, convoluted with a Gaussian distribution. Such a fit is displayed in Fig. 8. This gap feature appears both in measurements on the single crystals and on the polycrystals. Because the single crystal measurements probe the response only along one axis, while the polycrystal measurements average over all directions, we argue that the pseudogap must open up along the entire Fermi surface.

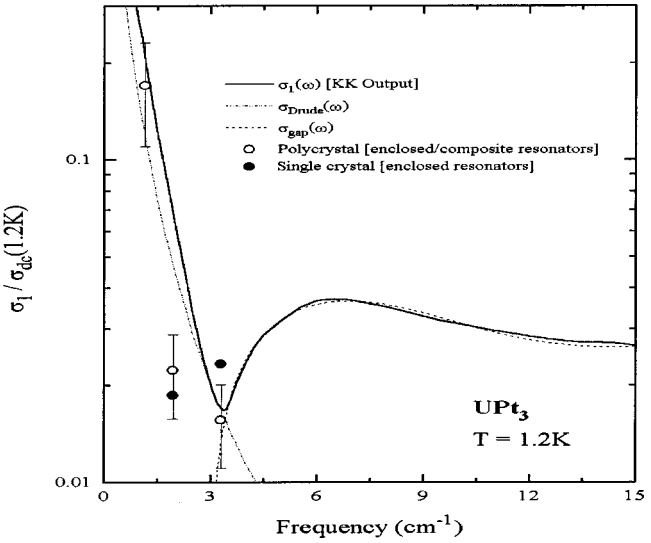

FIG. 8. The KK calculation (solid line) of the optical conductivity at 1.2 K, fitted to a Drude form $\sigma_{\mathrm{drude}}(\omega)$ and a pseudogap form $\sigma_{\mathrm{gap}}(\omega)$, as described in the text.

IV. CONCLUSIONS

The overall feature of the charge excitation spectrum of UPt_3 at low temperatures and frequencies is dramatically different from that of a renormalized Fermi liquid. We find a zero-energy mode coexisting with gapped charge excitations, the latter having an energy of the order of 1 meV. This feature appears in the temperature range where the resistivity displays a T^2 temperature dependence, and indicates that a renormalized Fermi liquid picture is inadequate in describing the thermodynamic and transport properties. The zero-energy mode has small spectral weight, in agreement with the enhanced thermodynamic quantities. The small spectral weight is also in full agreement with the magnitude of the London superconducting penetration depth.

The finite-energy mode centered around 1 meV is similar to what is expected for a fluctuating spin density wave state

with only short-range order;[30] such a state would lead to a pseudogap instead of a well-defined gap in the charge excitation spectrum. This suggests close connection to the short-range magnetic order observed by various experiments.[5–8] The pseudogap we observe indicates that the magnetic state develops as the consequence of a Fermi surface instability, a situation similar to that of a spin-density-wave (SDW) state.[30] A SDW state with *s*-wave symmetry is expected to lead to such features, but *d*-wave (electron-hole) pairing[32] also produces the features we observe.

In Fig. 9, we have displayed the optical gaps of three HF compounds with a magnetic ground state.[32,33] The increasing transition temperature is associated with an increased optical gap, in accordance to the simplest BCS expression of the gap $2\Delta = 3.5 k_B T_c$, indicated by the full line in Fig. 9. This would imply a Fermi-surface instability scenario for these materials. The magnetic properties suggest a more complicated state. The magnetic moment of a simple (*s*-wave) SDW state is given by[30]

$$\frac{\mu}{\mu_B} = \frac{\Delta_{\mathrm{SDW}}}{D_{\mathrm{ren}}} = \frac{\Delta_{\mathrm{SDW}} m_b}{D m^*} \tag{10}$$

where D is the unrenormalized bandwidth, $D_{\mathrm{ren}} = D(m_b/m^*)$ is the renormalized bandwidth, and m_b is the bare, unrenormalized band mass. Here we have assumed that not the unrenormalized, bare bandwidth D but the renormalized bandwidth D_{ren} is the relevant energy scale. This would imply a small moment in each case, and a moment which also depends on the gap and on the strength of renormalization. Using the unrenormalized bandwidth of 1 eV, Eq. (10) together with the effective-mass value we have derived before, leads to $\mu \sim 0.1 \mu_B$ in UPt_3, a magnetic moment significantly larger than that observed.[5–8] In UCu_5, on the other hand, a large moment of the order of μ_B is obtained in clear contrast with what one would obtain from Eq. (10). Clearly, the HF magnetic state of these materials is not fully understood.[34]

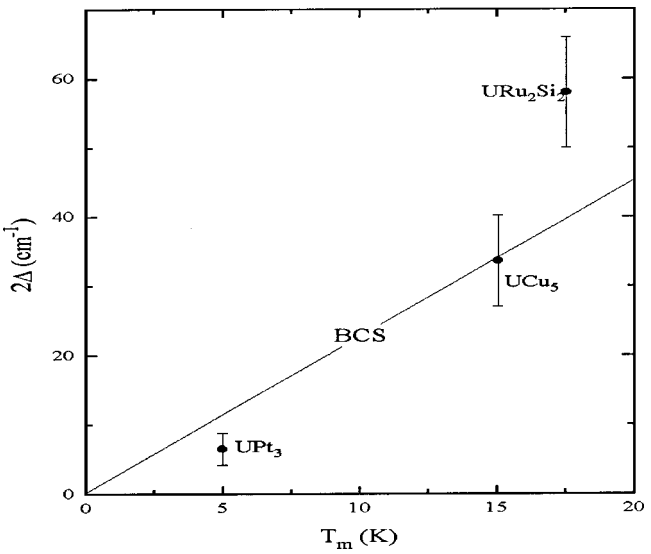

FIG. 9. Optical gaps of various heavy fermion materials with a magnetic ground state vs the transition temperatures for the onset of the magnetic state. The data for URu_2Si_2 and UCu_5 are taken from Ref. 33. The full line represents the BCS expression, $2\Delta = 3.5 k_B T_c$.

ACKNOWLEDGMENTS

We thank B. Maple for providing the samples used in this study, and P. Coleman, T. Ohashi, D. Pines, and A. Virosztek for useful discussions. This research was supported by National Science Foundation Grant No. DMR-9801816.

[1] R. Stewart, Rev. Mod. Phys. **56**, 755 (1984); P. A. Lee, T. M. Rice, J. W. Serene, L. J. Sham, and J. W. Wilkins, Comments Condens. Matter Phys. **12**, 99 (1986).

[2] G. Gruner, Adv. Phys. **23**, 941 (1974); G. Gruner and A. Zawadowski, Rep. Prog. Phys. **37**, 1497 (1974).

[3] L. Degiorgi, Rev. Mod. Phys. **71**, 687 (1999).

[4] K. R. Ott and Z. Fisk, in *Handbook on the Physics and Chemistry of Actinides*, edited by A. J. Freeman and G. H. Lander (North-Holland, Amsterdam, 1987).

[5] G. Aeppli, E. Bucher, C. Broholm, J. K. Kjems, J. Baumann, and J. Hufnagl, Phys. Rev. Lett. **60**, 615 (1988); S. M. Hayden, L. Taillefer, C. Vettier, and J. Flouquet, Phys. Rev. B **46**, 8675 (1992).

[6] R. H. Heffner, D. W. Cooke, A. L. Giorgi, R. L. Hutson, M. E. Schillaci, H. D. Rempp, J. L. Smith, J. O. Willis, D. E. Maclaughlin, C. Boekema, R. L. Lichti, J. Oostens, and A. B. Denison, Phys. Rev. B **39**, 11 345 (1989).

[7] P. H. Frings, D. Rinkin, and C. Vetties, J. Magn. Magn. Mater. **63**, 202 (1987).

[8] A. de Visser, R. J. Keizer, A. A. Menovsky, M. Mihalik, F. S. Tautz, J. J. M. Franse, B. Fak, N. H. van Dijk, J. Flouquet, J. Bossy, and S. Pujol, Physica B **230**, 49 (1997).

[9] F. Marabelli and P. Wachter, Physica B **163**, 224 (1990).

[10] F. Marabelli, G. Travaglini, P. Wachter, and J. J. M. Franse, Solid State Commun. **59**, 381 (1986).

[11] P. E. Sulewski, A. J. Sievers, M. B. Maple, M. S. Torikachvili, J. L. Smith, and Z. Fisk, Phys. Rev. B **38**, 5338 (1988).

[12] A. M. Awasthi, W. P. Beyermann, J. P. Carini, and G. Gruner, Phys. Rev. B **39**, 2377 (1989).

[13] W. P. Beyermann, A. M. Awasthi, J. P. Carini, and G. Gruner, J. Magn. Magn. Mater. **76**, 207 (1988).

[14] S. Donovan, A. Schwartz, and G. Gruner, Phys. Rev. Lett. **79**, 1401 (1997).

[15] A. Schwartz, M. Dressel, A. Blank, T. Csiba, G. Gruner, A. A. Volkov, B. P. Gorshunov, and G. V. Kozlov, Rev. Sci. Instrum. **66**, 2943 (1995).

[16] G. Gruner, in *Millimeter and Submillimeter Wave Spectroscopy of Solids*, edited by G. Gruner, Topics in Applied Physics, Vol. 74 (Springer-Verlag, Berlin, 1998), Chap. 4, pp. 111–166.

[17] O. Klein, S. Donovan, M. Dressel, and G. Gruner, Int. J. Infrared

Millim. Waves **14**, 2423 (1993); M. Dressel, O. Klein, S. Donovan, and G. Gruner, *ibid.* **14**, 2489 (1993).
[18] P. Tran and G. Gruner (unpublished).
[19] R. D. Lending, Proc. Natl. Electron. Conf. **11**, 395 (1955).
[20] F. Wooten, in *Optical Properties of Solids* (Academic, San Diego, 1972).
[21] A. de Visser, J. J. M. Franse, A. Menovsky, and T. T. M. Palstra, Physica B & C **127B**, 442 (1984).
[22] N. W. Ashcroft and N. D. Mermin, in *Solid State Physics* (Saunders College, Philadelphia, 1976).
[23] R. N. Gurzhi, Zh. Eksp. Tear. Fiz. **35**, 965 (1958) [Sov. Phys. JETP **8**, 673 (1959)]; P. S. Risenborough, Phys. Rev. B **27**, 5775 (1983).
[24] J. Schoenes and J. J. M. Franse, Phys. Rev. B **33**, 5138 (1986).
[25] M. Tinkham and R. A. Ferrell, Phys. Rev. Lett. **2**, 331 (1959).
[26] L. Taillefer, B. Ellman, B. Lussier, and M. Poirier, Physica B **230**, 327 (1997).
[27] C. M. Varma, K. Miyake, and S. Schmitt-Rink, Phys. Rev. Lett. **57**, 626 (1986).
[28] R. H. Heffner and M. R. Norman, Comments Condens. Matter Phys. **17**, 361 (1996).
[29] P. Y. Yu and M. Cardona, in *Fundamentals of Semiconductors* (Springer-Verlag, Berlin, 1996).
[30] G. Gruner, in *Density Waves in Solids* (Addison-Wesley, Reading, MA, 1994).
[31] V. Vescoli, L. Degiorgi, W. Henderson, G. Gruner, K. P. Starkey, and L. K. Montgomery, Science **281**, 1181 (1998).
[32] H. Ikeda and Y. Ohashi, Phys. Rev. Lett. **81**, 3723 (1998); D. A. Bonn, J. D. Garret, and T. Timusk, *ibid.* **61**, 1305 (1988).
[33] L. Degiorgi, S. Thieme, H. R. Ott, M. Dressel, G. Gruner, Y. Dalichaouch, M. B. Maple, Z. Fisk, C. Geibel, and F. Steglich, Z. Phys. B: Condens. Matter **102**, 367 (1997); L. Degiorgi, H. R. Ott, M. Dressel, G. Gruner, and Z. Fisk, Europhys. Lett. **26**, 221 (1994).
[34] P. W. Anderson, Adv. Phys. **46**, 3 (1997).